



**HAL**  
open science

## Freeze granulation and spray drying of mixed granules of Al<sub>2</sub>O<sub>3</sub>

M. Singlard, A. Paillassa, L. Ferres, Cécile Pagnoux, Anne Aimable

► **To cite this version:**

M. Singlard, A. Paillassa, L. Ferres, Cécile Pagnoux, Anne Aimable. Freeze granulation and spray drying of mixed granules of Al<sub>2</sub>O<sub>3</sub>. Powder Technology, 2022, 395, pp.280-289. 10.1016/j.powtec.2021.09.044 . hal-04741821

**HAL Id: hal-04741821**

**<https://unilim.hal.science/hal-04741821v1>**

Submitted on 13 Nov 2024

**HAL** is a multi-disciplinary open access archive for the deposit and dissemination of scientific research documents, whether they are published or not. The documents may come from teaching and research institutions in France or abroad, or from public or private research centers.

L'archive ouverte pluridisciplinaire **HAL**, est destinée au dépôt et à la diffusion de documents scientifiques de niveau recherche, publiés ou non, émanant des établissements d'enseignement et de recherche français ou étrangers, des laboratoires publics ou privés.



Distributed under a Creative Commons Attribution - NonCommercial 4.0 International License

# 1 Freeze granulation and spray drying of mixed granules 2 of Al<sub>2</sub>O<sub>3</sub>

3 M. Singlard<sup>1,2</sup>, A. Paillassa<sup>1</sup>, L. Ferres<sup>1</sup>, C. Pagnoux<sup>2</sup>, A. Aimable<sup>2</sup>

4 1 Institut de Recherche Technologique Saint Exupéry, Esplanade des arts et métiers, 33405 Talence,  
5 France

6 2 IRCER, Centre Européen de la Céramique, Université de Limoges, 12 rue Atlantis, 87068 Limoges,  
7 France

## 8 1. Introduction

9 Granulation techniques are widely used in many industrial sectors, and for various purposes. The  
10 pharmaceutical industry uses granulation for coating or encapsulation of active ingredients [1]. In the  
11 food industry, granulation provides additional properties such as aesthetic, shelf life, odor, taste, UV  
12 or moisture protection etc. In the ceramic industry, granulation is used to facilitate the flow of  
13 powders, and therefore their handling by dosers and conveyors. It also improves the pressability of  
14 the materials, and thus green density and densification rate for sintering. Another application is for  
15 the preparation of intimate ceramic-organic mixtures for specific processes such as Selective Laser  
16 Sintering [2–4]. Granulation techniques can also be used to improve bulk density and fluidity of  
17 nanoscale powders to increase their workability while maintaining their other properties as required  
18 to build nanostructured coating by plasma spraying [5,6]. In all these application, a good control of  
19 the granule size and morphology is required, as it impacts the green mechanical properties of the  
20 granules [7].

21 The spray drying process consists of pumping a suspension or a solution to a spray nozzle, then  
22 drying the resulting droplets in a chamber containing a stream of hot gas (usually air but could be  
23 nitrogen for oxidation-sensitive materials) and finally collecting with a cyclone (or other technique)  
24 the dry granules formed [1]. Depending on the way in which the suspension is atomized into fine  
25 droplets, a distinction is made between pressure nozzle atomizers, rotary atomizers and pneumatic  
26 atomizers [8]. The gas flow can be in the same direction as the spray (so-called co-current  
27 atomization) or in the opposite direction (so-called counter-current atomization). The shear rates  
28 experienced by the suspension during spraying can reach values as high as  $10^6 \text{ s}^{-1}$  [9]. To encapsulate  
29 a ceramic powder in a polymer, spray drying can be used as it has been the case with alumina, glass  
30 or silicon carbide powders [2–4,10]. The granule size increases with the suspension viscosity [9], solid  
31 content [11,12], surface tension [1], particle size [13], feed rate [1] and nozzle diameter [1]. It  
32 decreases with the density of spraying gas, atomization pressure [1] and, for rotary atomizers, with  
33 rotational speed and diameter of the rotating disc [8]. During the drying of the granules (after  
34 spraying), the species in solution tend to migrate with the liquid to the surface. This phenomenon  
35 leads to segregation of the species in solution, most of which are then found on the surface.  
36 Typically, this occurs when using suspensions with organic additives, such as binders. Although the  
37 binders have a certain affinity with the oxide surfaces, a large part of them is found in solution. For  
38 example, Baklouti et al. determined that the adsorption limit of polyvinyl alcohol (PVA) on the  
39 alumina surface is around  $0.6 \text{ mg/m}^2$  [14]. Therefore, when the amount is higher, the binder remains  
40 in solution and migrates to the surface of the droplets during drying. Binder segregation is promoted  
41 by a high binder content, a large amount of liquid, large granule and drop sizes, and a high solvent  
42 evaporation rate [15].

43 Freeze-granulation consists in spraying a suspension above a bath at very low temperature (usually  
44 liquid nitrogen) to freeze the droplets before they dry [16]. The extremely fast cooling rate allows the  
45 solvent (usually water) to solidify without crystallization. The frozen granules are then recovered and  
46 dried by lyophilization, i.e. liquid sublimation. Since the spraying method of the freeze granulation is

47 the same as these by atomization, all spraying parameters affecting the granules size are identical  
48 [17]. Granule density increases with solid content. Granule surface is smoother when the solid  
49 content of the suspension is higher. Freeze granulation can overpass the quality of spray drying when  
50 the product is sensitive to high temperature. In addition, due to fast freezing and lyophilisation, the  
51 granules are mainly spherical, contrary to spray drying [18]. Although more complex to implement,  
52 freeze granulation may be preferred to spray drying when the product to be treated is very sensitive  
53 to the high temperatures required for drying. In addition, it can be complex to obtain full and  
54 spherical granules by spray drying because of the migration phenomenon mentioned above, whereas  
55 freeze granulation ensures spherical, homogeneous and low density granules that is useful for dry  
56 pressing operation to achieve high green density (better pressability thanks to low granule density),  
57 high green strength (strength of a non-sintered ceramic) and better homogeneity [19]. When high  
58 homogeneity granules (multi-material granules) are required, as for nuclear applications [20] and  
59 transparent ceramics [21], freeze granulation is recommended. Freeze granulation could be useful  
60 for 3D printing techniques which used powder bed like binder jetting [22,23]. In addition, for  
61 hazardous powders, freeze granulation is a better option than spray drying because it is a dust-free  
62 process [24].

63 These previous studies have revealed the importance of some experimental parameters and their  
64 influence on the final granule size and their morphology. However, only trends are derived from  
65 these studies (size increases or decreases with a given parameter) and it is not possible to determine  
66 in advance the size of a granule using the characteristics of the suspension and the granulation  
67 process. In this paper we propose a new parameter called Pu (for pulverization number), able to  
68 predict the granule size through a multi-parameter approach, taking into account both slurry and  
69 process parameters. This study was conducted in the context of the formulation of mixed granules of  
70 alumina with a high content of organic binders to improve their plasticity at a medium temperature.  
71 Thus in a preliminary study the rheological behaviour of the suspensions was conducted to optimize

72 their formulations and better predict the influence of the relative concentrations of dispersant and  
73 binder to the alumina content.

## 74 2. Materials and methods

### 75 2.1. Materials

76 Alumina powder is supplied by Alteo, France, under the reference P172LSB. Specific surface area is  
77 measured at 8.6 m<sup>2</sup>/g (BET method) and the mean diameter at 0.4 μm (laser diffraction method).  
78 According to the supplier, the alumina content is 99.8%.

79 The dispersant used is an ammonium polymethacrylate (Darvan C-N, Vanderbilt) with molar mass of  
80 10-16 kg/mol.

81 Three organic additives of different molecular weight are used: polyethylene glycol (from 4 to 100  
82 kg/mol, named PEG-1 to PEG-3), polyethyloxazoline (from 50 to 500 kg/mol, named PEOx-1 to PEOx-  
83 5), and a rosin ester (RE). PEG and PEOx are water soluble in large proportion whereas RE is modified  
84 with a surfactant to make it dispersible in water.

85 The surface tension of the suspension is controlled thank to 0.04 v.% of a polyether-modified  
86 siloxane surfactant (BYK348, BYK Chemie).

87

### 88 2.2. Formulation of the suspensions and procedure for their preparation

89 Different formulations of suspensions were prepared by varying the concentration of the dispersant  
90 (X), the content of the organic additives (R) and the solid content (C), as defined below:

91 **-X is the dispersant content (mass of dispersant/surface of alumina), in mg/m<sup>2</sup>.** Since the  
92 dispersant adsorbs on the ceramic particles surface, the dispersant content in mg/m<sup>2</sup> is better suited  
93 than in wt.%.

94 -R is the volume percent of organic additive on the total dry matter (organic additives +  
95 alumina)  $R = \frac{C_{add}^{vol}}{C_{add}^{vol} + C_{alumina}^{vol}}$ , in vol.%. R is a key parameter, which represents the ratio of  
96 organic binder in the final granule.

97 -C is the volume percent of dry matter in the suspension ( $C = \frac{C_{add}^{vol} + C_{alumina}^{vol}}{C_{water}^{vol}}$ , in vol.%)

98 The procedure for the preparation of these suspensions is as follows (also detailed in Supplementary  
99 Materials). The powder is added gradually in an aqueous solution of dispersant while stirring. The  
100 suspension is then deagglomerated by an ultrasonic treatment and then, placed for 15 hours on  
101 rollers to allow dispersant adsorption on the powder surface. This suspension is referred to as the  
102 mother suspension. The additive (PEG or PEOx) is solubilized in water under agitation at room  
103 temperature prior to its introduction into the mother suspension to ensure a better homogeneity.  
104 The RE additive is already supplied as an aqueous dispersion by the manufacturer and is used as  
105 received. In the case of an additive mixture, the polymers are introduced in descending order of  
106 molar mass, because the dissolution of the additives of high molecular weight is easier when the  
107 solution is less viscous. Once the additive solution is introduced into the mother suspension, the  
108 sample is stirred for 90 minutes and then the surfactant is introduced. After a further 90 minutes of  
109 homogenization, the surface tension and viscosity of the suspension are measured. Finally, the  
110 sample can be granulated, either by freeze granulation or spray drying.

111

### 112 2.3. Granulation of the suspensions: freeze granulation and spray drying

113 Freeze granulation (Figure 1a) is carried out using a PowderPro apparatus equipped with an external  
114 mixing nozzle with a 1.4 mm opening. The suspension feed rate and the air velocity are set  
115 respectively at 36 mL/min, and from 87 to 204 m/s. The distance between the nozzle and the liquid  
116 nitrogen is about 20-30 mm. This distance is an order of magnitude greater than the calculated

117 distance (using the ratio of the dynamic pressures of the fluid and air) of jet breakage under the  
118 experimental conditions used [25]. Granules are freeze-dried (Beta 2-8 LDplus, Christ) for 18 hours.

119 The suspension is poured into one beaker and the liquid nitrogen into another. Both are kept under  
120 agitation by magnetic stirrers. A peristaltic pump drives the suspension into the nozzle. The nozzle is  
121 connected to compressed air, the pressure of which is adjusted in order to vary the air velocity at the  
122 nozzle outlet. The nozzle is mounted at the top of the beaker in its center. When the suspension  
123 beaker is empty, the airflow is stopped. A metal tray supplied with the freeze dryer is filled with  
124 liquid nitrogen until boiling stops, meaning that the tray has reached the temperature of liquid  
125 nitrogen. With a ladle, the frozen granules are collected and poured into the tray. During the  
126 transfer, the granules remain covered with liquid nitrogen to ensure that they remain frozen. Once  
127 all the frozen granules are recovered, the tray is inserted into the freeze dryer and the sublimation  
128 cycle begins. At the end of the cycle, the freeze-dried granules are collected in a vial for further  
129 analysis.

130 Spray drying (Figure 1b) is carried out with two equipments named hereafter SD1 (Buchi Mini Spray  
131 Dryer, 190) and SD2 (Buchi Mini spray Dryer B-290). These equipments are lab-scale machines and  
132 are very similar in their principle and use. They are from different generation, working thanks to an  
133 internal mixing nozzle. The drying air flow is co-current and the dried granules are collected with a  
134 cyclone. The inlet temperature is set at 190-220 °C in order to achieve an outlet temperature  
135 (measured just before the cyclone) of 90-120 °C. In internal mixing nozzles, suspension and air are  
136 ejected through the same orifice. Thus, even knowing the air and suspension flow rates (in m<sup>3</sup>/s), it is  
137 not possible to simply deduce the air velocity (in m/s) because the cross-sectional area (in m<sup>2</sup>) is not  
138 equal to the nozzle diameter (due to the simultaneous passage of the suspension and air through this  
139 diameter). The air velocity is therefore not indicated, but the pressure in the air circuit is kept  
140 constant for all experiments.

141

## 142 2.4. Characterization techniques

143 The rheological properties of the suspensions are measured by a rheometer (ARG2, TA Instruments)  
144 with a cone-plate geometry (titanium, 60 mm, 2°) from 10 to 300 s<sup>-1</sup> in shear rate at 20 °C. All the  
145 viscosity values presented in this article are taken at 100 s<sup>-1</sup>.

146 The Wilhelmy method is used to measure the surface tension of the suspension (DCAT11,  
147 Dataphysics). The plate is made of platinum-iridium alloy. The Wilhelmy method assumes that the  
148 contact angle between the plate and the sample is (near) zero. The platinum-iridium alloy produces a  
149 zero contact angle with most liquids. To avoid pollution that could change the contact angle value,  
150 the plate is cleaned in the flame of a Bunsen burner before each measurement. The surface tension  
151 is measured continuously until the standard deviation of the last 50 points is below 0.03 mN/m. The  
152 surface tension measurement is the mean of these 50 points.

153 The size distribution of the granules is measured by laser diffraction (Mastersizer 2000, Malvern),  
154 using a dry route with a 1 bar pressure. For each sample, the powder is fed into the equipment  
155 continuously, and three measurements are averaged.

156 The morphology of the granules is observed by scanning electron microscopy (SEM, Jeol IT300 LV)  
157 with secondary electrons, a 5 kV accelerating voltage and 8-10 mm working distance. Before  
158 observation, samples are metallized by a 15 nm thick platinum layer.

## 159 3. Results and discussions

### 160 3.1. Rheological behaviour of the suspensions for the granulation process

161 Ceramic suspensions with organic additives exhibit generally a non-Newtonian behaviour which can  
162 be described by the Herschel-Bulkley law (Equation 1).

163 **Equation 1**

$$164 \tau = \tau_0 + K\dot{\gamma}^n$$



165 Where  $\tau$  is the shear stress (Pa),  $\dot{\gamma}$  the shear rate ( $s^{-1}$ ),  $\tau_0$  the yield stress (Pa),  $n$  the flow index and  $K$   
166 a constant. The yield stress is the minimal shear stress required to initiate flow. The flow index  
167 represents the deviation from a Newtonian behavior: if  $n < 1$ , the suspension is shear thinning and if  
168  $n > 1$ , the suspension is shear thickening.

169 Nine suspensions were formulated with the additive PEOx-5, by varying the concentration of  
170 dispersant  $X$  from 0.1 to 1.0  $mg/m^2$ , the organic content  $R$  from 20 to 50 vol%, and the solid content  
171  $C$  from 15 to 30 vol.%. From these experiments, the variations of viscosity and flow index were  
172 modeled using polynomials of degree 2 (least squares fitting). All available polynomials, using any  
173 number of monomials (from 1 to 7) were calculated and, for each property (viscosity and flow index  
174 with each additive), the best polynomial was selected. All the selected models use only two of the  
175 three variables ( $X$ ,  $R$  or  $C$ ), which allows a representation in graphs where the two variables are  
176 arranged in abscissa and ordinate. A colour scale (blue for the lowest value and red for the highest)  
177 represents the value of the viscosity or the flow index. The isovalue curves are represented in black.

178 The viscosity and the flow index measured are reported in Figure 2 (black dots) (details in table S1 in  
179 Supplementary materials). A model has been adjusted by the best polynomial of degree 2 (using the  
180 method of least squares). This model presents an adjusted R-square superior to 95%.

181 We can deduce from this model that the viscosity of the suspensions varies from 25 to 1000 mPa.s  
182 (Figure 2a) and is not dependent on the dispersant content ( $X$ ) in the measuring range (0.1 to 1.0  
183  $mg/m^2$ ). Baklouti *et al.* [26] and Cesarano *et al.* [27] find that the adsorption of polymethacrylate  
184 onto the alumina surface is maximal around 0.36  $mg/m^2$  but it seems that the viscosity remains low  
185 also for higher or lower values. Otherwise, the higher the organic content on dry matter ( $R$ ), and the  
186 solid content ( $C$ ), the higher the suspension viscosity. When the organic fraction of dry matter is high  
187 ( $R$  large), the increase in viscosity with dry matter content is faster. If the dry matter is 26% organic  
188 ( $R=26\%$ ), the viscosity increases from 62 mPa.s to 146 mPa.s (+135% increase) when the dry  
189 matter/water ratio (i.e.  $C$ ) increases from 21% to 30%. For  $R = 44\%$ , the viscosity increases from 168

190 to 628 mPa.s (+274% increase) over the same C range (20 to 30%). Therefore, the organic part of the  
191 suspension has a high impact on its viscosity.

192 The flow index of these suspensions ranges from 0.86 to 1 (Figure 2b), which means that the  
193 suspensions containing PEOx5 are all shear thinning. The flow index is not affected by the dry matter  
194 concentration (C), and only by the composition of the dry matter (R) and the dispersant content (X).  
195 However, R has only a moderate impact on the flow index as shown by the quasi-vertical isovalue  
196 curves in the figure. The flow index evolution with dispersant concentration (X) is non-linear with a  
197 maximum for about 0.7 mg/m<sup>2</sup> (Figure 2b), which corresponds to a newtonian behaviour ( $n = 1$ ). This  
198 type of evolution has already been observed by Zhou *et al.* [28].

199 Nine suspensions were also formulated with the resin RE, by varying the concentration of dispersant  
200 X from 0.1 to 1.0 mg/m<sup>2</sup>, the organic content R from 20 to 50 vol%, and the solid content C from 40  
201 to 60 vol.%. The viscosity and the flow index measured are reported in Figure 3 (black dots) (details in  
202 table S1 in Supplementary materials), and a model adjusted in the same conditions.

203 The viscosity of the suspensions containing RE is much lower than the one measured with PEOx-5 in  
204 the whole range, as it varies from about 5 to 35 mPa.s (Figure 3a). It depends mainly on the dry  
205 matter concentration (C) and the dispersant content (X), whereas it is not affected by the  
206 composition of the dry matter (R), which means that RE and alumina have the same impact on it. For  
207 a same dry matter concentration (C), a lower amount of dispersant produces a lower viscosity.  
208 Finally, the low viscosity values obtained (15 mPa.s for C = 40 %) show that alumina dispersed with  
209 ammonium polymethacrylate and RE are highly compatible.

210 The flow index of the suspensions containing RE varies from 0.74 to 1.0 (Figure 3b), corresponding to  
211 a shear thinning behaviour. Again, as for the viscosity, the composition of the dry matter (R) has no  
212 impact on this parameter. The higher the dispersant content (X) and the higher the dry matter  
213 content (C), the more shear thinning the suspensions are.

214 This preliminary study allows a good prediction of the rheological behaviour of the suspensions  
215 containing different organic additives. A wide range of concentrations could be explored through a  
216 simple polynomial modeling, combining the influence of organics concentration and the total solid  
217 content. This is an original and efficient approach to optimize the formulations for a given ceramic  
218 process in a liquid route such as granulation (freeze granulation and spray drying).

219

### 220 3.2. Suspension behaviour during freeze granulation

221 In the following, we make a focus on some limitations which are observed for the freeze-granulation  
222 of suspensions containing organics with the higher molecular weight (PEG-3). With 5 vol.% of PEG-3,  
223 no granule is obtained and a large amount of thick filament are observed (Figure 4a) whose diameter  
224 is measured at 25  $\mu\text{m}$  (mean of 10 measurements). By reducing the solid content, some granules  
225 could be produced with a lower amount of thinner (11  $\mu\text{m}$ ) filaments (Figure 4b). By reducing the  
226 polymer content and increasing the alumina content, thus conserving a close value for the viscosity  
227 (from Figure 4c to Figure 4d), spherical granules are obtained with a low content of filament.

228 Figure 5 shows the granules obtained with suspensions at the same concentrations of alumina and  
229 polymer, but with PEG of different molecular masses. The filaments are only observed with the  
230 higher molecular mass (PEG-3), no filaments are produced for the two lower molar masses of PEG  
231 polymer (PEG-1 and PEG-2).

232 In the freeze granulation process, the liquid jet is pulverized by the high speed air. Due to the surface  
233 tension, each fragment forms spherical droplets, which become granules after freeze-drying.  
234 However, polymer solution jets have a different behaviour from Newtonian liquids due to the  
235 polymer chains elongation during stretching taking place during spraying. Depending on the  
236 formulation, several centimeters-long filaments can be produced. The formation and stability of  
237 these filaments have already been studied [29,30]. The filaments have a natural tendency to become

238 thinner over time. Oliveira and McKinley have found that the decay in the filament radius (and  
239 therefore breakage when radius becomes equal to zero) is slower with higher molecular weight and  
240 polymer concentration [31]. Thus, if the molar mass and concentration of the polymer are  
241 inadequate, the filament does not have time to resorb before impact with liquid nitrogen in this  
242 study, like with PEG-3.

243

### 244 3.3. Model of prediction of the granule size obtained by freeze granulation and 245 spray drying

246 Laser granulometry is suitable to measure the granule size distribution, as shown in Figure 6. In all  
247 the experiments done either by spray drying or freeze granulation, the size distribution is single-  
248 mode. Therefore the granule size of a batch is reduced to its  $d_{50}$  (median particle size in volume) in all  
249 the following results shown in this paper. We can also observe that in any case, for all the  
250 formulations, the granule size is always higher by freeze granulation than by spray drying. This is  
251 explained because the droplets are frozen very rapidly in the liquid nitrogen, and recovered through  
252 lyophilisation, leading to very small differences between the droplet size and the granule size. During  
253 spray drying, the droplets encounter a shrinkage because of the drying occurring in the hot chamber,  
254 and their final size is much smaller.

255 During the granulation process, the inlet liquid (suspension) is disrupted by a high velocity airflow to  
256 produce drops that can be disrupted themselves to produce smaller drops. Three stresses are  
257 considered for a liquid drop in a gas stream [32]:

- 258 – The spraying stress  $P_s$ , related to the relative velocity of the liquid with the gas (dynamic  
259 pressure) (Equation 2).
- 260 – The stress related to the surface tension  $P_\gamma$ , related to the increase of the surface area,  
261 creating an opposing force to the fragmentation (Equation 3).

262 – Under the spraying stress, drop is deformed. Due to the viscosity of the liquid drop, a viscous  
263 stress is created  $P_\eta$  (Equation 4).

264 **Equation 2**

$$265 \quad P_s \propto \rho_g u^2$$

266 **Equation 3**

$$267 \quad P_\gamma \propto \gamma_l / d$$

268 **Equation 4**

$$269 \quad P_\eta \propto \frac{\eta_l}{d} \sqrt{\frac{P_s}{\rho_l}}$$

270 With  $\rho$  the density (kg/m<sup>3</sup>),  $\gamma$  the surface tension (N/m),  $\eta$  the dynamic viscosity (Pa.s),  $u$  the relative  
271 velocity of air and liquid (m/s) and  $d$  the drop diameter (m). Subscripts  $g$  and  $l$  are related to the gas  
272 and liquid phase, respectively.

273 Thus, to promote the spraying, the spraying stress must be maximal (**process** parameter), whereas  
274 viscosity and surface tension must be minimized (**formulation** parameters). From these three  
275 stresses, one can build two dimensionless numbers  $Re^*$  and  $We^*$ , representing the competition  
276 between the disruptive spraying force and the viscosity (Equation 5) and surface tension force  
277 (Equation 6).

278 **Equation 5**

$$279 \quad Re^* = \frac{P_s}{P_\eta} = \frac{d_n \sqrt{\rho_g \rho_l} u}{\eta_l}$$

280 **Equation 6**

$$281 \quad We^* = \frac{P_s}{P_\gamma} = \frac{d_n \rho_g u^2}{\gamma_l}$$

282  $Re^*$  is similar to the Reynold number, considering the density of the two phases (gas and liquid).  $We^*$   
283 is similar to the Weber number, with the characteristics of the gas ( $\rho_g$ ) and the liquid ( $\gamma_l$ ). Surface  
284 tension and viscous stresses use the diameter of the drop as the characteristic length. However, in  
285 the case of spraying ( $Re^*$  and  $We^*$ ), the diameter of the nozzle ( $d_n$ ) is preferred. The higher  $Re^*$  and  
286  $We^*$ , the higher the spraying stress, compared to the viscous and surface tension stresses  
287 respectively. Thus, the final droplet size is smaller with higher  $Re^*$  and  $We^*$ . From  $Re^*$  and  $We^*$ , a  
288 unique dimensionless number is created and called pulverization number  $Pu$  (Equation 7).

289 Equation 7

$$290 \quad Pu = \sqrt{Re^* \times We^*} = \frac{P_s}{\sqrt{P_\eta P_\gamma}} = \frac{d_n \rho_g^{3/4} \rho_l^{1/4} u^{3/2}}{\sqrt{\gamma_l \eta_l}}$$

291 This number represents the competition between the disruptive forces (from dynamic pressure) and  
292 the forces opposed to the deformation (from viscosity and surface tension).

293 Different suspensions were formulated with variable concentrations of alumina powder and organic  
294 additives at different concentrations. Their viscosity, surface tension and density were measured,  
295 and used to calculate the corresponding pulverization number  $Pu$  (see table S2 in Supplementary  
296 Material). In addition, some suspensions were sprayed with higher air velocity  $u$ . The air velocity is  
297 estimated from the volume of air ejected in a given time and the diameter of the nozzle. Figure 7  
298 shows the variation of the mean size of granules produced by freeze-granulation with the  
299 pulverization number. This figure clearly proves that the granule size is only related to the  
300 pulverization number, and does not depend on the nature of the additive. The  $R^2_{aj}$  coefficient,  
301 related to the quality of the correlation, is equal to 88 %. The constant coefficient of the model  
302 represents the effect of the process parameters, which are not taken into account in  $Pu$ , like feed  
303 rate of the suspension, the travel time of drops and so on.

304 The relationship between the mean granule size and  $Pu$  is valid over a wide range of size and  $Pu$ ,  
 305 granule size varying from 22  $\mu\text{m}$  with RE, up to 420  $\mu\text{m}$  with PEG-2 and PEG-3. Therefore, by using  
 306 this new parameter, one can have a very high degree of prediction on the final size of the granules  
 307 obtained by freeze-granulation, and thus a very robust and efficient method to adapt the parameters  
 308 of the formulation and/or the process. Although the equation produces good results with the  
 309 experimental data,  $Pu$  does not take into account several variables that can have an impact on the  
 310 size of the granules: geometry of the nozzle (beyond its diameter), distance between the nozzle and  
 311 the liquid nitrogen, pumping speed of the suspension. It is likely that other equipment would result in  
 312 variations in the value of the coefficients, including the constant shown in Figure 7.

313

314 This new parameter has to be adapted in the case of spray drying. In freeze granulation, the size of  
 315 the droplets is close to size of the granules, because they are frozen very rapidly and recovered by  
 316 sublimation. Whereas during the spray drying process, the droplets encounter a shrinkage because of  
 317 the drying occurring in the hot chamber. Indeed  $Pu$  is related to the drop size, which is equal to the  
 318 granule size in freeze granulation but not in spray drying. In addition, two different spray dryers were  
 319 used in this study, which leads to a variation in numerous parameters: size of the drying chamber,  
 320 velocity of the drying air, nozzle size, efficiency of the cyclone and so on. Consequently, the  $Pu$   
 321 parameter is splitted into two parts: the first one ( $Mat$ ) is related to the material properties and the  
 322 second one ( $Pro$ ) is related to the equipment.

323 **Equation 8**

$$324 \quad Mat = \frac{Pu}{(C_{alumina}^{vol} + C_{add}^{vol})d_b u^{3/2}} = \frac{\rho_g^{3/4} \rho_l^{1/4}}{(C_{alumina}^{vol} + C_{add}^{vol})\sqrt{\gamma_l \eta_l}}$$

325 **Equation 9**

$$326 \quad Pro = \begin{cases} 1 & \text{with spray drier SD1} \\ 2 & \text{with spray drier SD2} \end{cases}$$

327 Equation 10

$$328 \quad Pu' = Mat^{\beta_1} \times Pro^{\beta_2}$$

329 The process parameters in Pro are not explicit (Equation 9), and  $\beta_1$  and  $\beta_2$  are two constants to be  
330 determined. Pu' number is fitted to the data, the results are shown in Figure 8 (see table S3 in  
331 Supplementary Material for the numerical values). R<sup>2</sup>aj is 71%, which gives a relatively good  
332 agreement with the data, but not excellent. Actually, it is expected that the drying has a large impact  
333 on the granule size, and the granule shape (hollow spherical, full spherical, donut-like). Full spherical  
334 shape is favoured by a low inlet temperature, a low content and molar mass of polymer, a high  
335 ceramic loading, a high yield shear stress [9], and a high viscosity [33]. In addition to the granule  
336 shape, segregation of the polymer in solution may occur. Segregation is favoured by a high polymer  
337 content, a high liquid content, a large drop and a high evaporation rate [15]. Granule shape has a  
338 direct impact on their size, which explains the lower quality of the fitting compared to the freeze  
339 granulation data with Pu.

340

### 341 3.4. Granule morphology

342 Figure 9 compares the morphology of some granules obtained by freeze granulation and spray  
343 drying. Freeze-dried granules are mainly full and spherical whereas spray-dried ones have a greater  
344 variety of morphologies: one can find hollow are donut-like shapes as dense and full for a same  
345 product. That variability is in agreement with the difficulty to predict the spray-dried granule size  
346 without considering the drying as presented at Figure 8. Freeze-dried granules are smoother and  
347 present a lower compacity. Indeed, the droplets do not shrink during the freeze-drying and the  
348 volume initially occupied by water becomes porosity.

349 Freeze granulation leads to typical morphologies with polymer-coated areas and others with  
350 apparent porosities (Figure 10 a). Below a notched surface polymer films are no longer visible. Spray



351 dried granule surface can be polymer-coated or not, depending on the formulation of the suspension  
352 (Figure 10 b-c).

#### 353 4. Conclusions

354 This comparative study of spray drying and freeze granulation was conducted for the preparation of  
355 mixed granules of submicronic alumina with a high content of polymeric binder. First, the variation of  
356 the viscosity of the ceramic suspensions filled with a high molecular weight polymer or with a  
357 dispersed rosin ester was studied. The polymer content has a very large impact on the viscosity but  
358 not on the flow index. In comparison, the use of rosin ester leads to very low viscosities, even at high  
359 dry matter contents.

360 Suspensions with varying viscosities (7-208 mPa.s), densities (1.31-1.76) and surface tensions (23-40  
361 mN/m) were then granulated. The first observations reveal the importance of the content and the  
362 molar mass of the binder. It turns out that too high elasticity of the suspension leads to granulation  
363 failure. It is therefore essential to select an appropriate molar mass / additive concentration  
364 combination. Then by studying the forces involved, it was possible to propose a new and unified  
365 dimensionless number called pulverization number  $Pu$  to predict the size of the granules produced  
366 by freeze granulation from simple material (density, viscosity, surface tension) and process (velocity)  
367 data. This parameter is valid over a wide range of granule size (22 to 420  $\mu\text{m}$ ).  $Pu$  has been adjusted  
368 for spray drying, to partially take into account evaporative drying. However, the model is less  
369 effective in predicting granule size. Presumably, this difference is due to the fact that the constructed  
370 dimensionless number  $Pu$  is rather a predictor of droplet size and not of granule size. These two sizes  
371 are equal in the case of freeze granulation because the droplets are frozen and the water is removed  
372 without any shrinkage. On the contrary, by spray drying, the evaporation can lead to a significant  
373 shrinkage or not, depending on the morphology of the granule obtained. The amplitude of the  
374 shrinkage has not been taken into account, which leads to a greater difficulty in predicting the size of  
375 the sprayed granules. To confirm this hypothesis, the drop size produced by atomization could be

376 measured in a future study and compared to the prediction made using Pu. In addition,  
377 reproducibility tests will be needed to confirm the results presented in this article.

378 The freeze-dried granules are mostly full and spherical with high degree of porosity, which  
379 corresponds to the place occupied by the water before freeze-drying of the frozen droplet. The  
380 spray-dried granules are of various shapes, even for the same batch. The morphologies found are the  
381 dense spherical shape, the hollow shape and the donut shape.

## 382 Nomenclature

383 Latin letters

C	Volume percent of dry matter in the suspension
$C_{alumina}^{vol}$	Volume percent of alumina in the suspension
$C_{add}^{vol}$	Volume percent of organic additive in the suspension
R	Volume percent of organic additive on the total dry matter
d	Drop diameter (m)
$d_{50}$	Mean diameter by volume (m)
$d_n$	Nozzle diameter (m)
K	Constant in Herschel-Bulkley model
Mat	Part of Pu' related to material properties
n	Flow index
Pro	Part of Pu' related to process properties
$P_s$	Spraying stress (Pa)
Pu	Pulverization number
Pu'	Modified pulverization number
$P_\gamma$	Stress related to surface tension (Pa)

$P_{\eta}$	Viscous stress (Pa)
$Re^*$	Modified Reynolds number
$u$	Gas velocity (m/s)
$We^*$	Modifier Weber's number
$X$	Dispersant content relative to alumina surface (kg/m <sup>2</sup> )

384

385 Greek letters

$\beta_1$	Fitting constant in the expression of $Pu'$
$\beta_2$	Fitting constant in the expression of $Pu'$
$\dot{\gamma}$	Shear rate (s <sup>-1</sup> )
$\eta$	Dynamic viscosity (Pa.s)
$\rho$	Density (kg/m <sup>3</sup> )
$\tau$	Shear stress (Pa)
$\tau_0$	Yield stress (Pa)

386

### 387 Acknowledgment

388 The authors would like to thank Safran Ceramics for the financial support (and in particular Gautier  
389 Mécuson) and Jérôme Kiennemann from Alteo (France) for the kindly supplying of alumina powder  
390 used in this research. We would also like to thank François Louvet, Associate Professor at the  
391 University of Limoges, for the technical expertise in construction the experimental matrices for the  
392 rheology study and for the subsequent data processing.

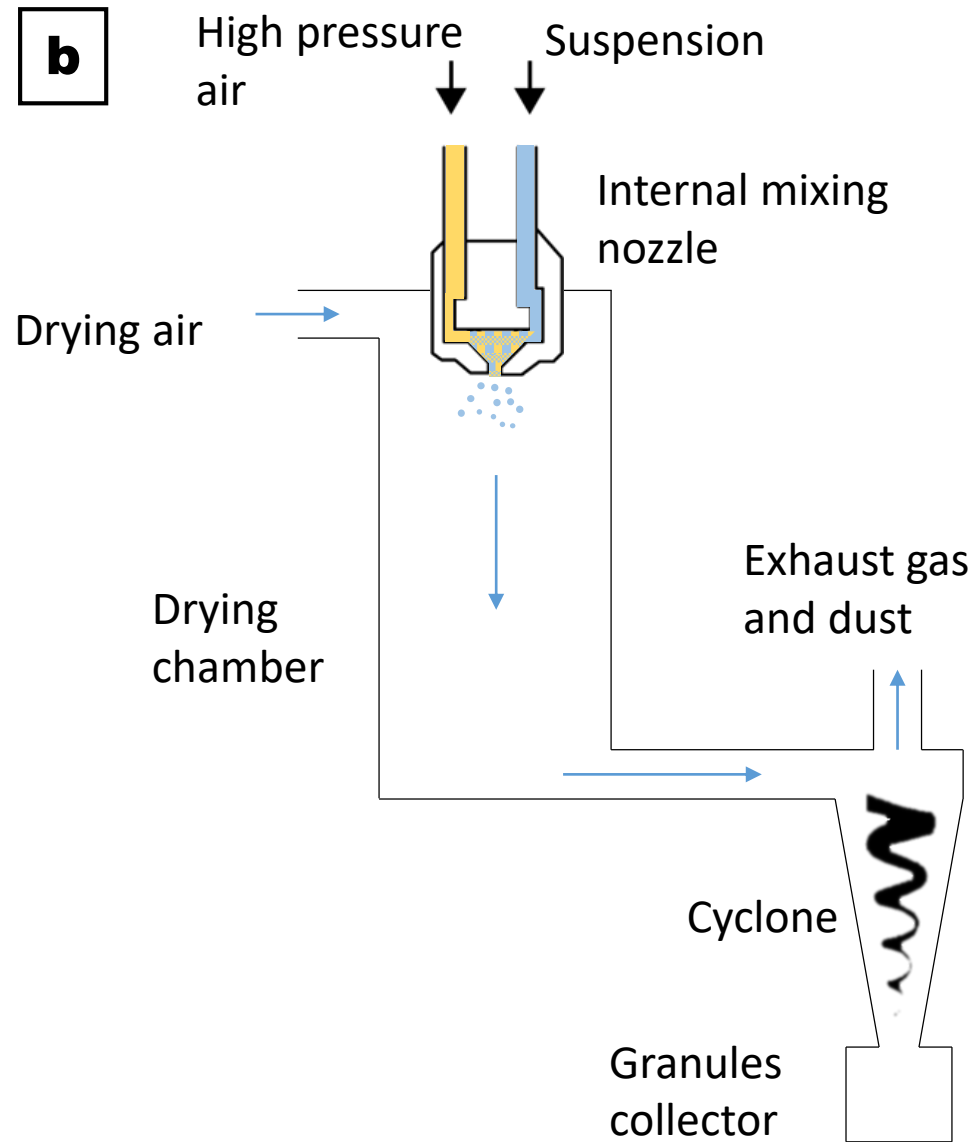
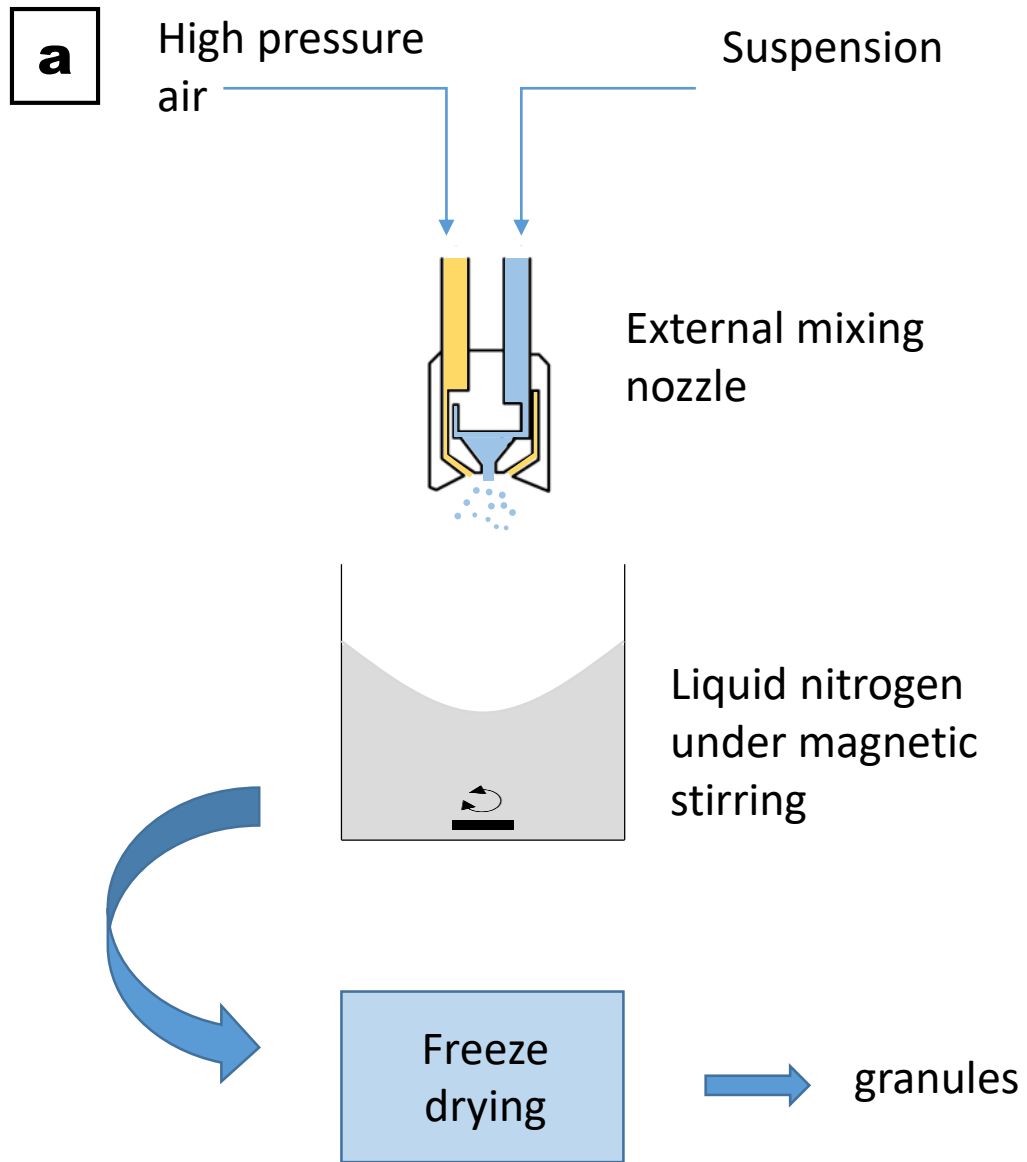
393 **References**

- 394 [1] A. Sosnik, K.P. Seremeta, Advantages and challenges of the spray-drying technology for the  
395 production of pure drug particles and drug-loaded polymeric carriers, *Advances in Colloid and*  
396 *Interface Science*. 223 (2015) 40–54.
- 397 [2] K. Subramanian, N. Vail, J. Barlow, H. Marcus, Selective laser sintering of alumina with polymer  
398 binders, *Rapid Prototyping Journal*. 1 (1995) 24–35.
- 399 [3] J.C. Nelson, N.K. Vail, J. Barlow, J.J. Beaman, D.L. Bourell, H.L. Marcus, Selective laser sintering  
400 of polymer-coated silicon carbide powders, *Industrial & Engineering Chemistry Research*. 34  
401 (1995) 1641–1651.
- 402 [4] N.K. Vail, J.W. Barlow, Effect of polymer coatings as intermediate binders on sintering of  
403 ceramic parts, in: 1991.
- 404 [5] C. Lee, H. Choi, C. Lee, H. Kim, Photocatalytic properties of nano-structured TiO<sub>2</sub> plasma  
405 sprayed coating, *Surface and Coatings Technology*. 173 (2003) 192–200.
- 406 [6] E. Sanchez, E. Bannier, V. Cantavella, M.D. Salvador, E. Klyatskina, J. Morgiel, J. Grzonka, A.R.  
407 Boccaccini, Deposition of Al<sub>2</sub>O<sub>3</sub>-TiO<sub>2</sub> Nanostructured Powders by Atmospheric Plasma Spraying,  
408 *Journal of Thermal Spray Technology*. 17 (2008) 329–337.
- 409 [7] J.L. Amoros, V. Cantavella, J.C. Jarque, C. Feliu, Fracture properties of spray-dried powder  
410 compacts: Effects of granule size, *Journal of the European Ceramic Society*. 28 (2008) 2823–  
411 2834.
- 412 [8] J.-M. Haussonne, C. Carry, P. Bowen, J. Barton, Atomisation, in: *Traité Des Matériaux.*  
413 *Céramiques et Verres : Principes et Techniques d'élaboration*, Presses Polytechniques et  
414 Universitaires Romandes, 2005: pp. 198–201.
- 415 [9] W.J. Walkers, J.S. Reed, Influence of Slurry Parameters on the Characteristics of Spray-Dried  
416 Granules, *Journal of the American Ceramic Society*. 82 (1999) 1711–1719.
- 417 [10] N.K. Vail, J.W. Barlow, Microencapsulation of Finely Divided Ceramic Powders, in: *International*  
418 *Solid Freeform Fabrication Symposium*, 1990.

- 419 [11] N. Vail, J.W. Barlow, Ceramic structures by selective laser sintering of microencapsulated, finely  
420 divided ceramic materials, in: 1992.
- 421 [12] A. Stunda-Zujeva, Z. Irbe, L. Berzina-Cimdina, Controlling the morphology of ceramic and  
422 composite powders obtained via spray drying - A review, *Ceramics International*. 43 (2017)  
423 11543–11551.
- 424 [13] P. Ramavath, R. Papitha, M. Ramesh, P.S. Babu, R. Johnson, Effect of primary particle size on  
425 spray formation, morphology and internal structure of alumina granules and elucidation of  
426 flowability and compaction behavior, *Processing and Application of Ceramics*. 8 (2014) 93–99.
- 427 [14] S. Baklouti, T. Chartier, J.F. Baumard, Binder Distribution in Spray-Dried Alumina Agglomerates,  
428 *Journal of the European Ceramic Society*. 18 (1998) 2117–2121.
- 429 [15] Y. Zhang, X. Tang, N. Uchida, K. Uematsu, Binder surface segregation during spray drying of  
430 ceramic slurry, *Journal of Materials Research*. 13 (1998) 1881–1887.
- 431 [16] K. Rundgren, O. Lyckfeldt, M. Sjostedt, Improving Powders With Freeze Granulation, *Ceramic*  
432 *Industry*. 153 (2003) 40–44.
- 433 [17] S. Shanmugam, Granulation techniques and technologies: recent progresses, *Bioimpacts*. 5  
434 (2017) 55–63. <https://doi.org/10.15171/bi.2015.04>.
- 435 [18] M. Vicent, E. Sanchez, T. Molina, M.I. Nieto, R. Moreno, Comparison of freeze drying and spray  
436 drying to obtain porous nanostructured granules from nanosized suspensions, *Journal of the*  
437 *European Ceramic Society*. 32 (2012) 1019–1028.
- 438 [19] B.P.C. Raghupathy, J.G.P. Binner, Spray Granulation of Nanometric Zirconia Particles, *Journal of*  
439 *the American Ceramic Society*. 94 (2011) 42–48.
- 440 [20] F. La Lumia, L. Ramond, C. Pagnoux, G. Bernard-Granger, Fabrication of homogenous pellets by  
441 freeze granulation of optimized  $\text{TiO}_2\text{-Y}_2\text{O}_3$  suspensions, *Journal of the European Ceramic*  
442 *Society*. 39 (2019) 2168–2178.
- 443 [21] M. Stuer, Z. Zhao, P. Bowen, Freeze granulation: Powder processing for transparent alumina  
444 applications, *Journal of the European Ceramic Society*. 32 (2012) 2899–2908.

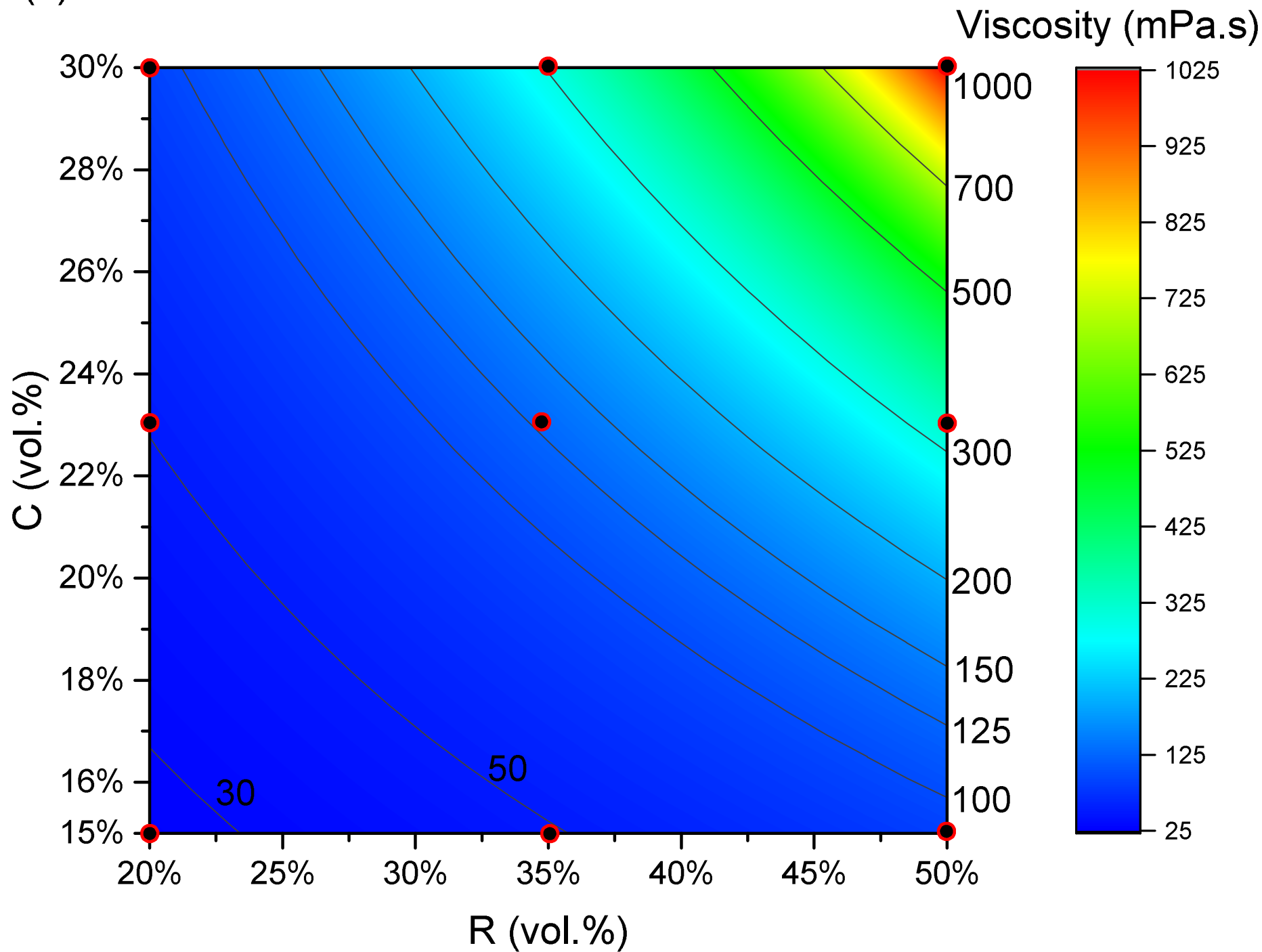
- 445 [22] G. Miao, W. Du, M. Moghadasi, Z. Pei, C. Ma, Ceramic binder jetting additive manufacturing:  
446 Effects of granulation on properties of feedstock powder and printed and sintered parts,  
447 Additive Manufacturing. 36 (n.d.) 101542.
- 448 [23] W. Du, G. Miao, L. Liu, Z. Pei, C. Ma, Binder jetting additive manufacturing of ceramics  
449 feedstock powder preparation by spray freeze granulation, in: Proceedings of the AMSE 2019,  
450 2019: pp. MSEC2019-3001.
- 451 [24] F. La Lumia, L. Ramond, C. Pagnoux, P. Coste, F. Lebreton, J.-R. Sevilla, G. Bernard-Granger,  
452 Dense and homogeneous MOX fuel pellets manufactured using the freeze granulation route,  
453 Journal of the American Ceramic Society. 103 (2020) 3020–3029.
- 454 [25] J. Ferguson, N. Hudson, B. Warren, The break-up of fluids in an extensional flow field, Journal of  
455 Non-Newtonian Fluid Mechanics. 44 (1992) 37–54.
- 456 [26] S. Baklouti, J. Bouaziz, T. Chartier, J.F. Baumard, Binder burnout and evolution of the  
457 mechanical strength of dry-pressed ceramics containing poly(vinyl alcohol), Journal of the  
458 European Ceramic Society. 21 (2001) 1087–1092.
- 459 [27] J. Cesarano, A. Aksay, A. Bleier, Stability of aqueous  $\alpha$ -Al<sub>2</sub>O<sub>3</sub> suspensions with poly (methacrylic  
460 acid) polyelectrolyte, Journal of the American Ceramic Society. 71 (1988) 250–255.
- 461 [28] M. Zhou, K. Huang, D. Yang, X. Qiu, Development and evaluation of polycarboxylic acid hyper-  
462 dispersant used to prepare high-concentrated coal–water slurry, Powder Technology. 229  
463 (2012) 185–190.
- 464 [29] V.M. Entov, E.J. Hinch, Effect of a spectrum of relaxation times on the capillary thinning of a  
465 filament of elastic liquid, Journal of Non-Newtonian Fluid Mechanics. 72 (1997) 31–53.
- 466 [30] S.L. Anna, G.H. McKinley, Elasto-capillary thinning and breakup of model elastic liquids, Journal  
467 of Rheology. 45 (2001) 115–138.
- 468 [31] M.S. Oliveira, G.H. McKinley, Iterated stretching and multiple beads-on-a-string phenomena in  
469 dilute solutions of highly extensible flexible polymers, Physics of Fluids. 17 (2005) 071704.

- 470 [32] J.O. Hinze, Fundamentals of the Hydrodynamic Mechanism of Splitting in Dispersion Processes,  
471 AIChE Journal. 1 (1955) 289–295.
- 472 [33] D.-J. Kim, J.-Y. Yung, Granule performance of ironia/alumina composite powders spray-dried  
473 using polyvinyl pyrrolidone binder, Journal of the European Ceramic Society. 27 (2007) 3177–  
474 3182.

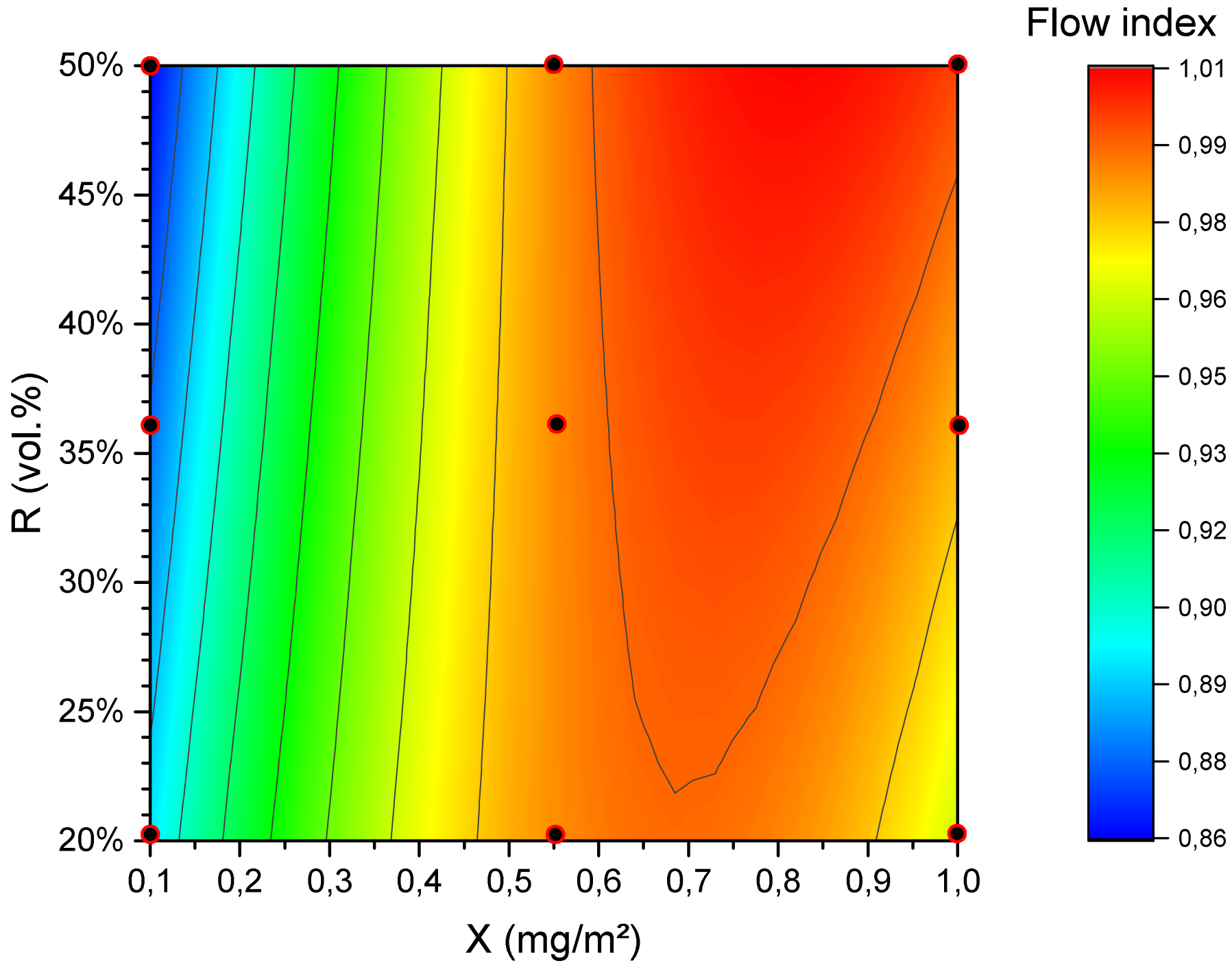


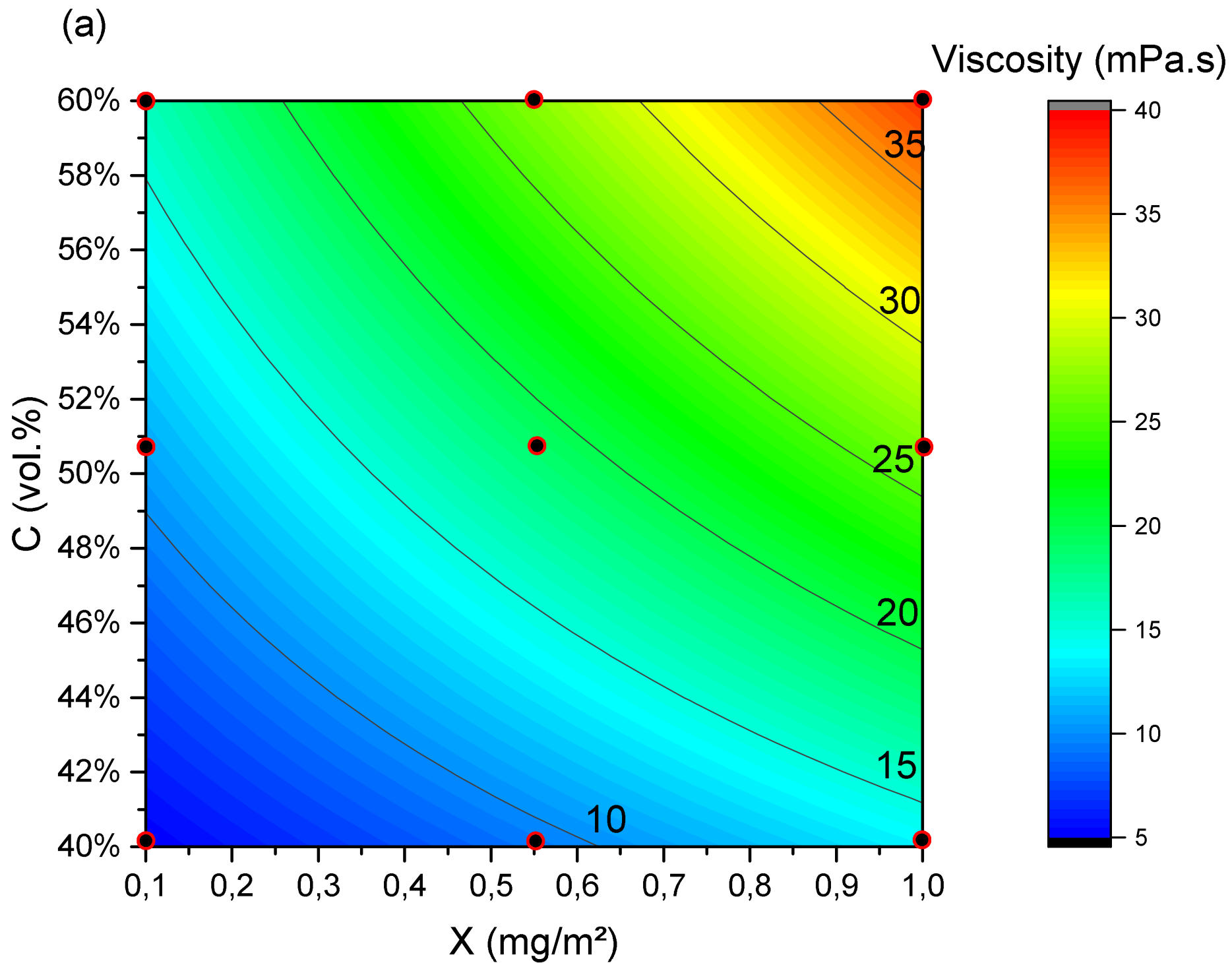


(a)

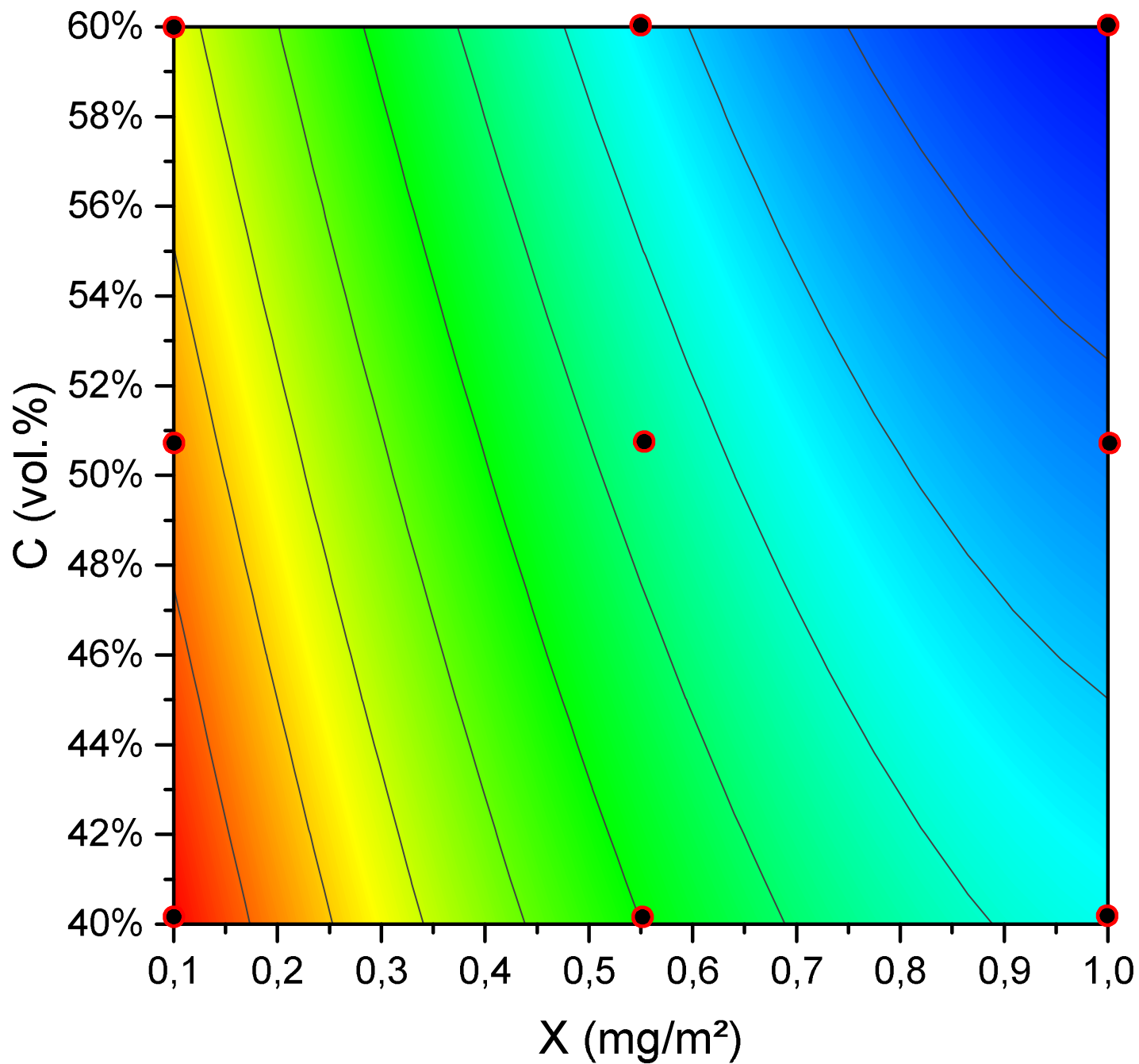


(b)

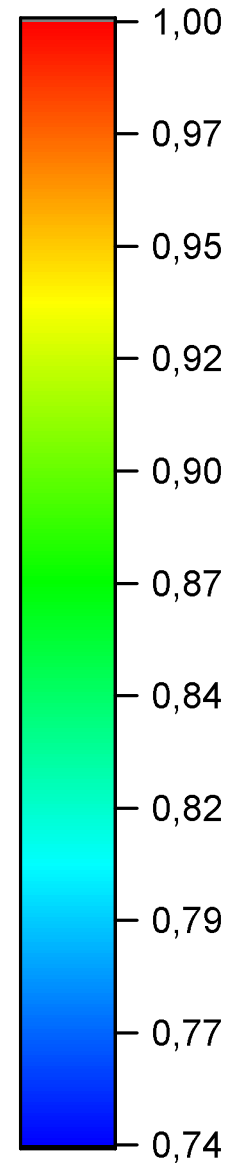




(b)

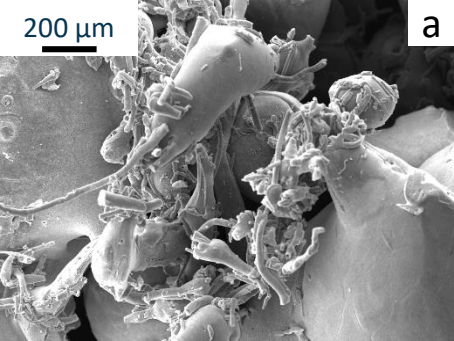


Flow index



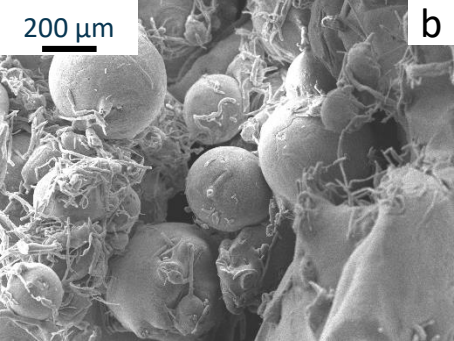
200  $\mu\text{m}$

a



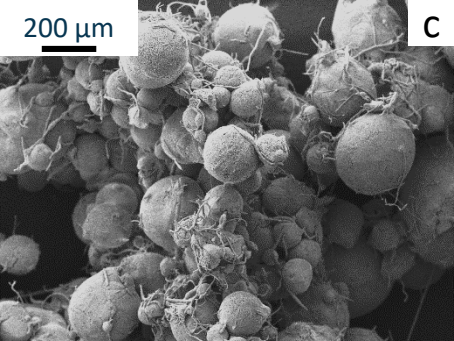
200  $\mu\text{m}$

b



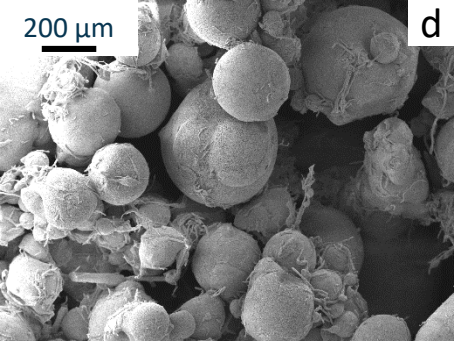
200  $\mu\text{m}$

C



200  $\mu\text{m}$

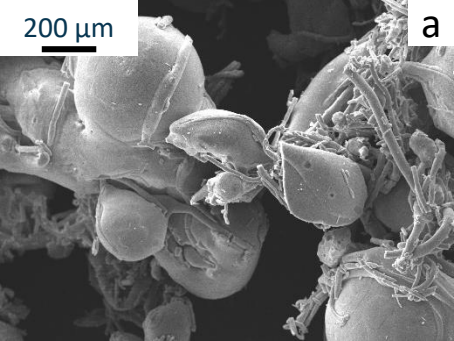
d





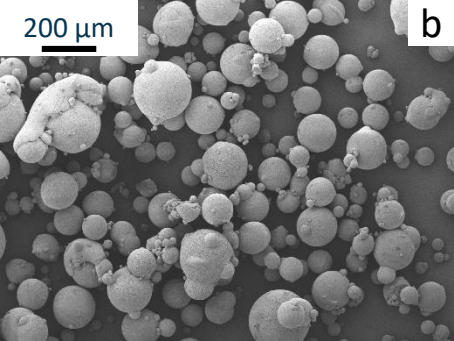
200  $\mu\text{m}$

a



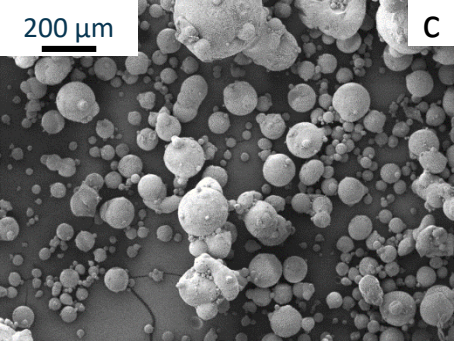
200  $\mu\text{m}$

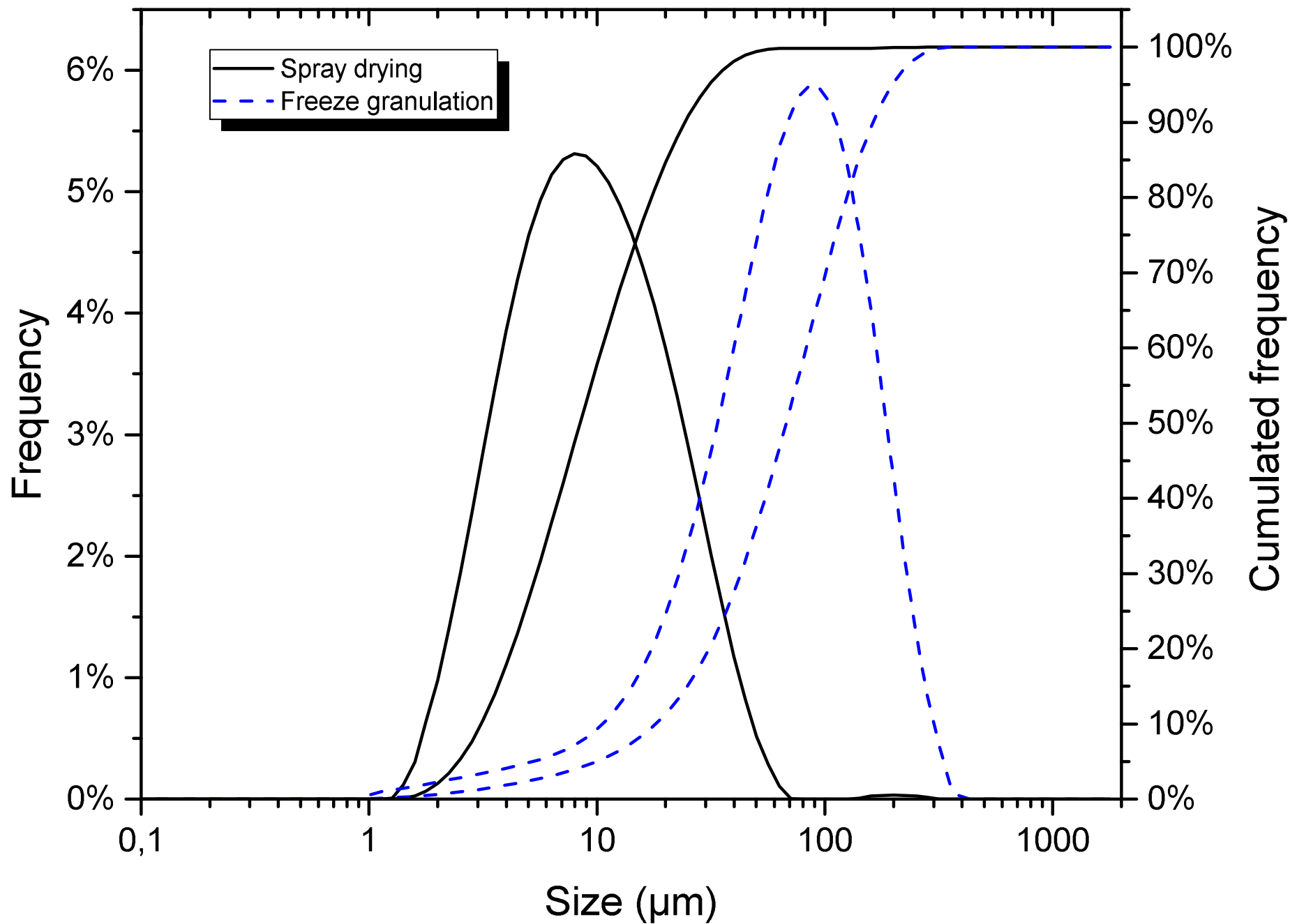
b

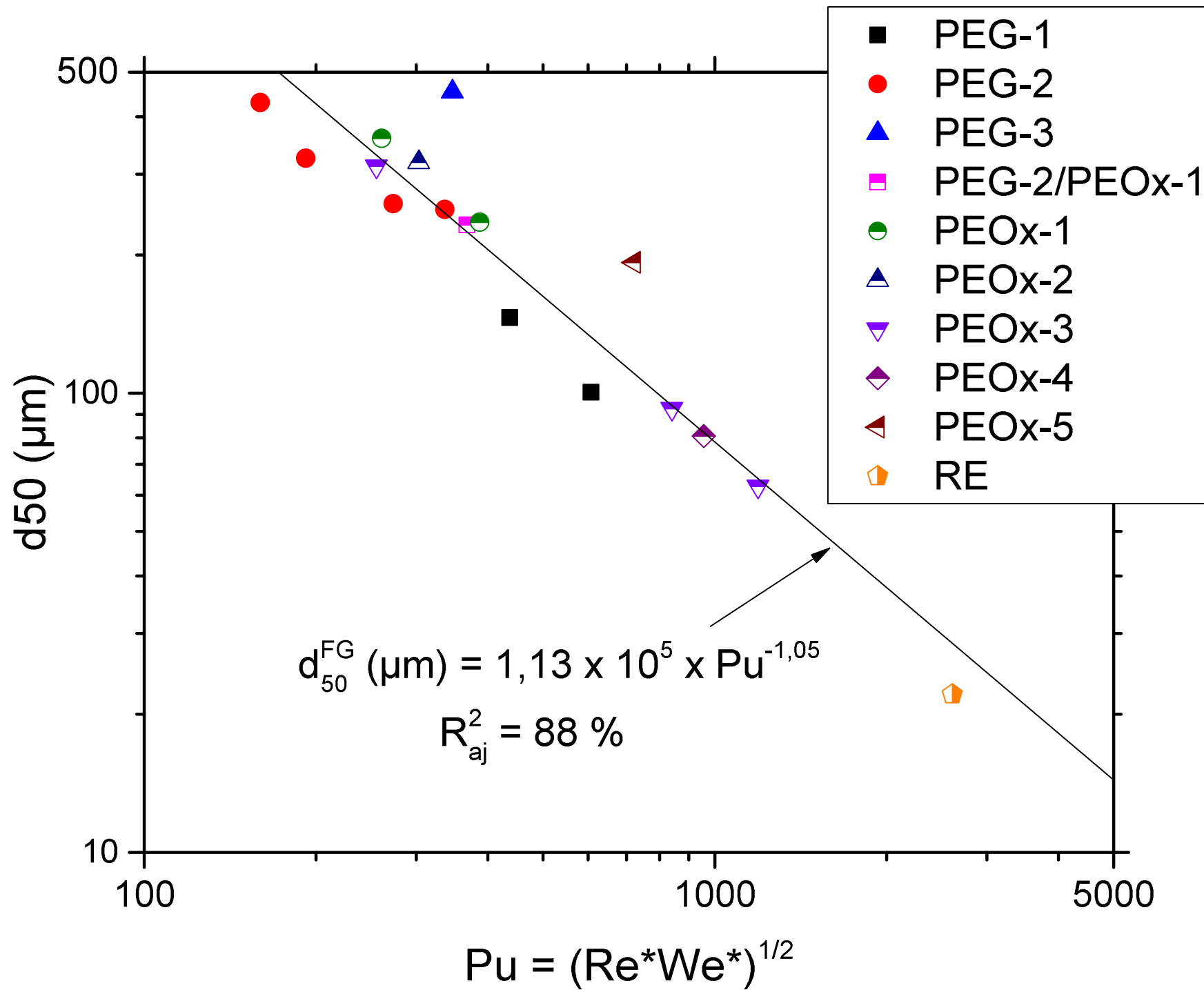


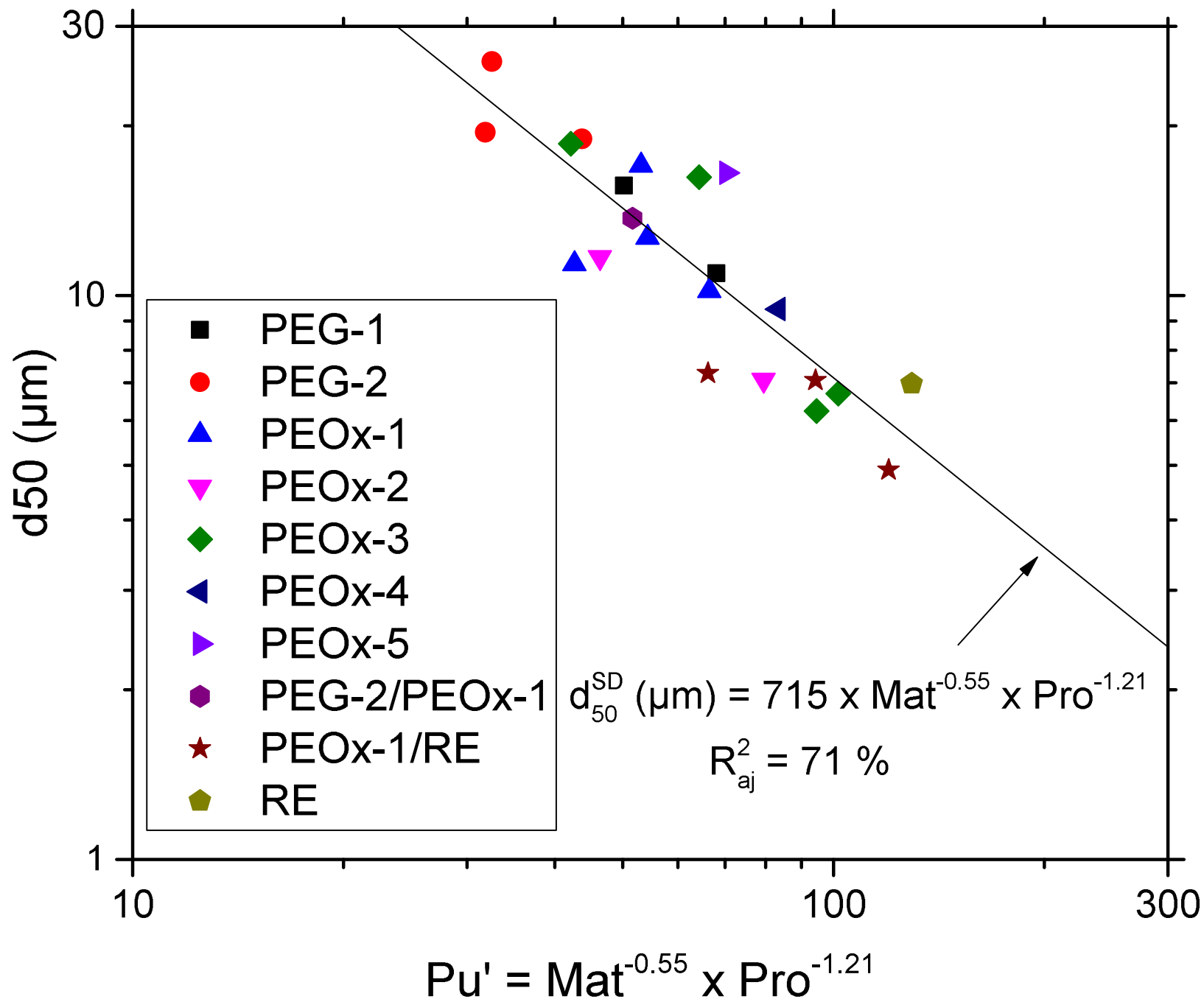
200  $\mu\text{m}$

C



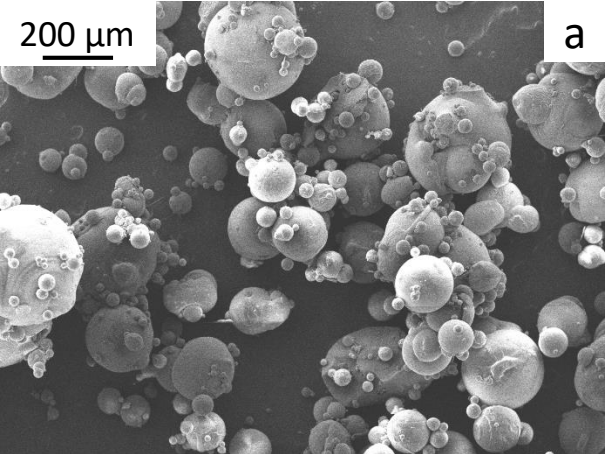






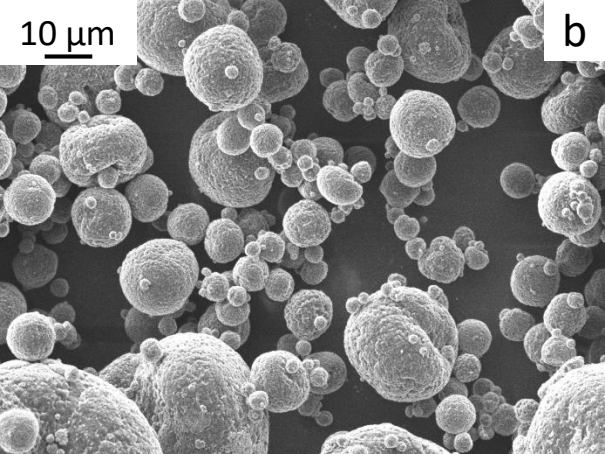
200  $\mu\text{m}$

a



10  $\mu\text{m}$

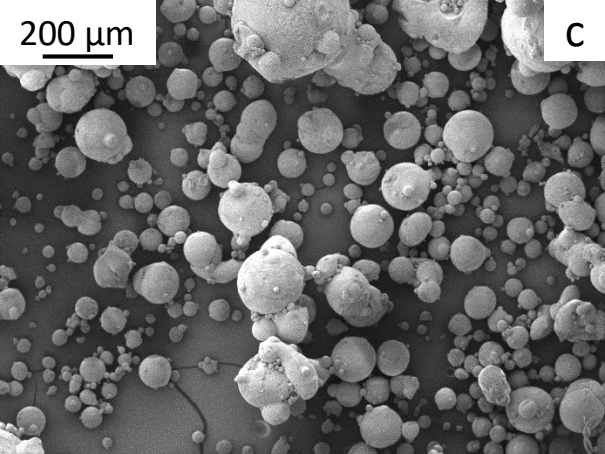
b





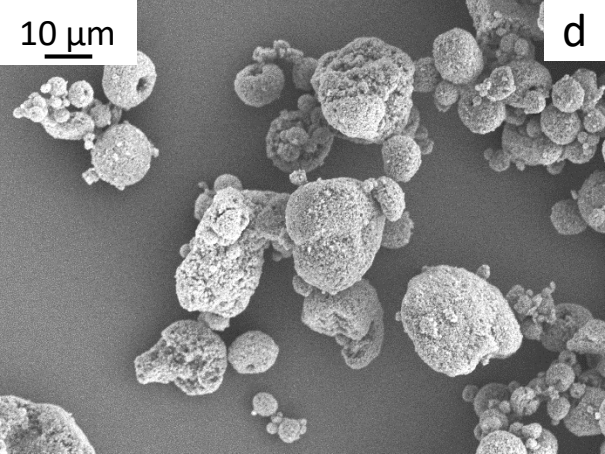
200  $\mu\text{m}$

C



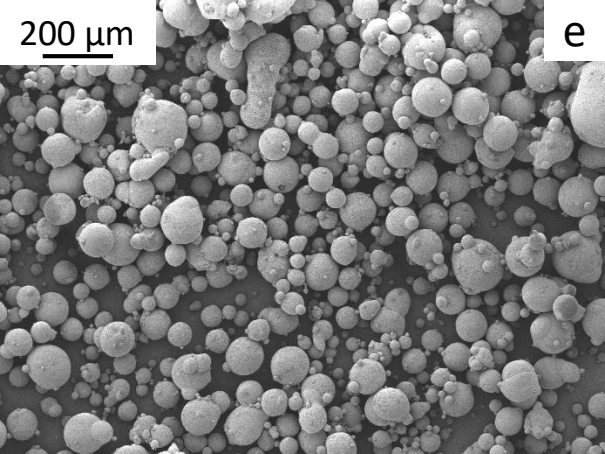
10  $\mu\text{m}$

d



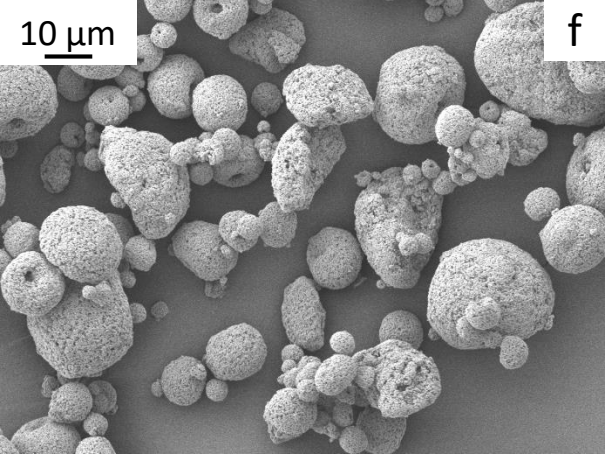
200  $\mu\text{m}$

e



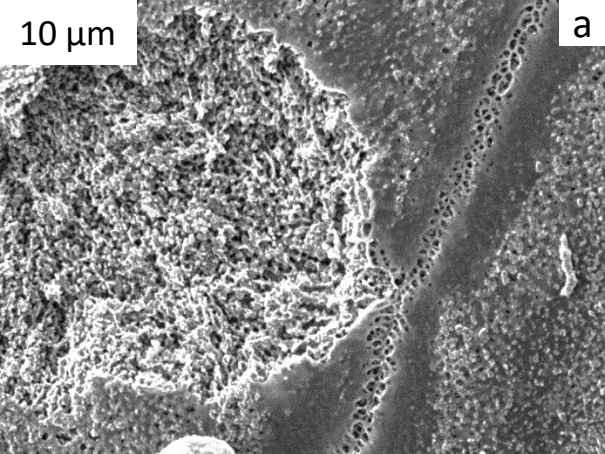
10  $\mu\text{m}$

f



10  $\mu\text{m}$

a



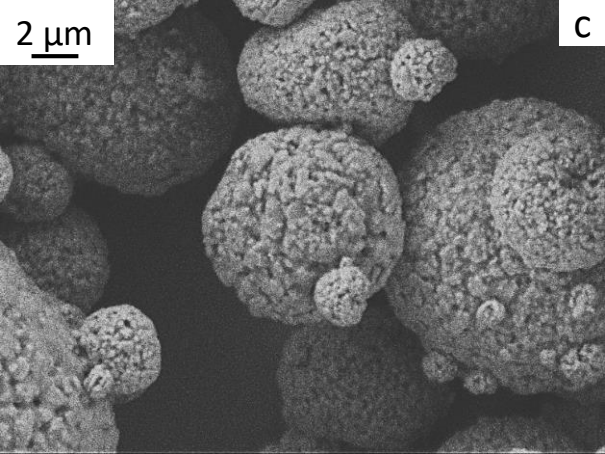
2  $\mu\text{m}$

This scanning electron micrograph (SEM) shows a collection of spherical particles with a highly textured, porous surface. The particles vary in size, with several prominent ones in the center and foreground. The surface morphology is characterized by irregular, interconnected protrusions and recesses, giving it a rough, cauliflower-like appearance. A scale bar in the top left corner indicates a length of 2 micrometers. The background is dark, highlighting the three-dimensional structure of the particles.

b

2  $\mu\text{m}$

C



# Production of mixed alumina granules by freeze-granulation and spray drying and highlights on size

## Methodology



Develop models to predict the viscosity of the suspensions



Construct an original dimensionless number from theoretical consideration

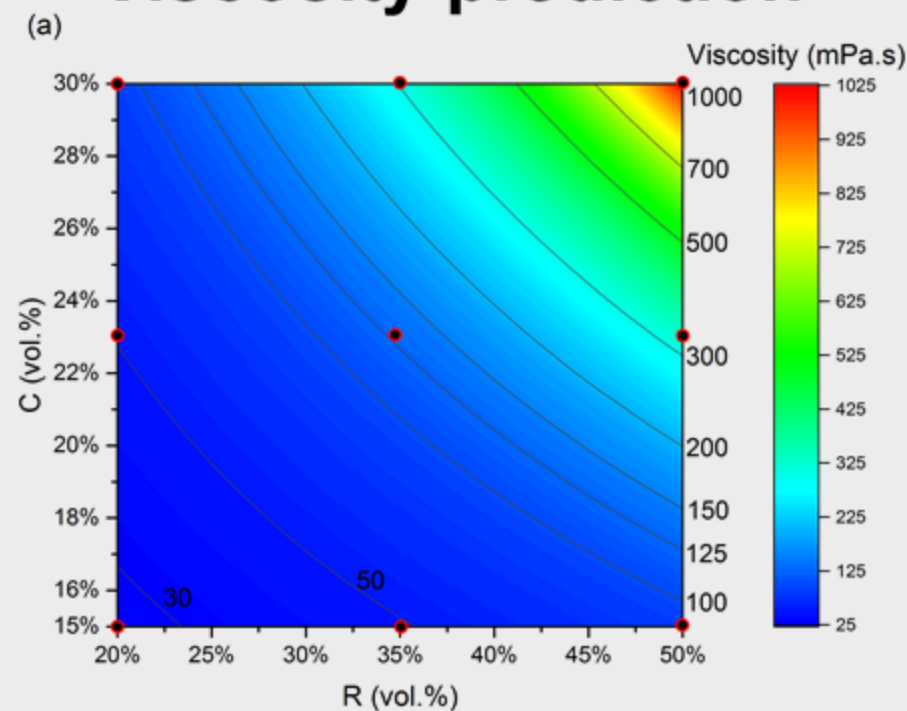
$$Pu = \frac{d_n \rho_g^{3/4} \rho_l^{1/4} u^{3/2}}{\sqrt{\gamma_l \eta_l}}$$



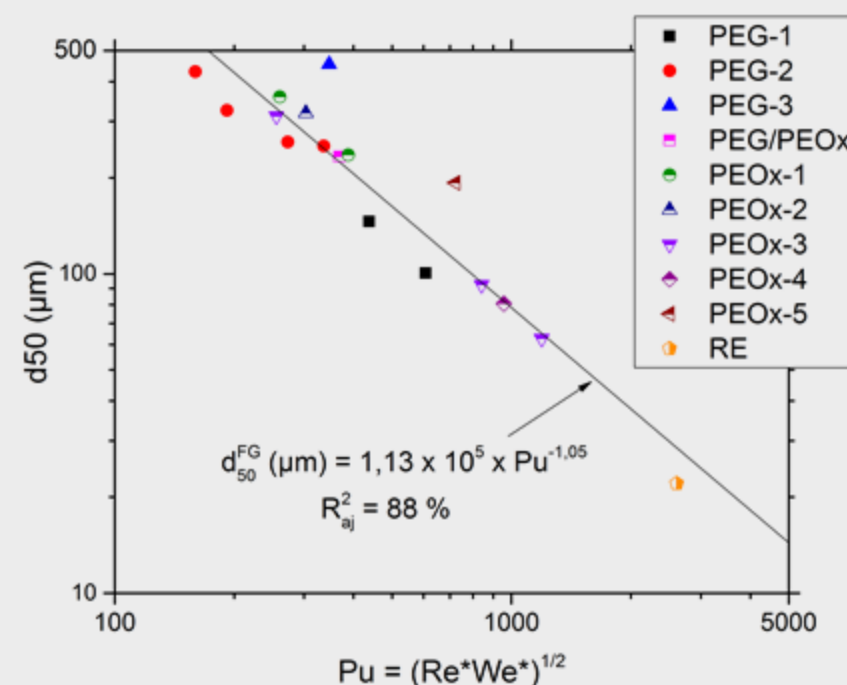
Analyse granule morphology

## Results

### Viscosity prediction



### Granule size prediction



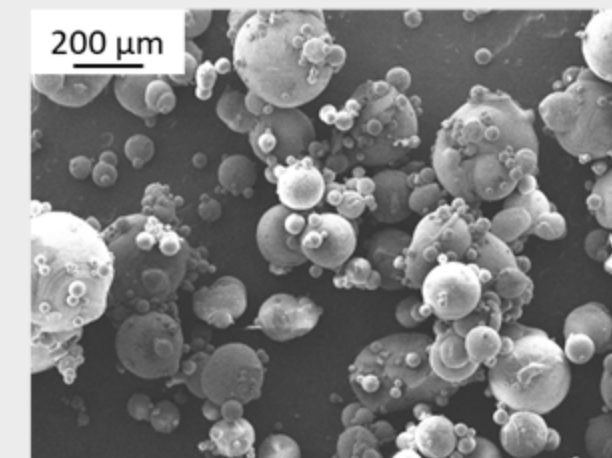
Good agreement between data and models



Bigger and more spherical granules by freeze granulation

### Morphology

#### Freeze-granulation



#### Spray drying

